

Efficient training of photonic quantum generative models

Felix Gottlieb, Rawad Mezher, Brian Ventura, Shane Mansfield, and Alexia Salavrakos

Quandela, 7 Rue Léonard de Vinci, 91300 Massy, France

The topic of generative learning has gained traction within the field of quantum machine learning, in particular with the advent of train-on-classical, deploy-on-quantum methods. This approach exploits the properties of intermediate-complexity circuits whose training can be simulated classically efficiently, but that generally require quantum hardware for the corresponding sampling problem. Quantum linear optics possess similar properties, which allows us to propose an efficient training procedure for photon-native quantum generative models based on the maximum mean discrepancy, where the deployment of the model corresponds to the task of boson sampling. We provide numerical results, propose datasets, and we also explore how initialization strategies and ansatz choice affect the training.

1 Introduction

The field of quantum machine learning (QML) is faced with two main challenges: training quantum models efficiently and at scale; and identifying practically useful problems for which quantum models outperform classical ones – ideally, showing the model is non-dequantizable. As highlighted in [1], no work to date fulfills all criteria. However, noteworthy results in this direction include the first example of a rigorous speedup in QML [2], the guarantee of backpropagation scaling for the training of a specific family of circuits [3], as well as frameworks and examples for formal learning separations [4, 5].

In the context of generative learning, the recent work of [6] proposes a compelling approach that targets the problem of training QML models efficiently and at scale. The authors present a generative model based on parametrized Instantaneous Quantum Polynomial (IQP) circuits [7], for which it is known that expectation values of observables can be approximated classically efficiently through the den Nest algorithm [8]. Importantly, in the related work of [9], the authors consider a loss function often used in generative learning called the Maximum Mean Discrepancy (MMD) [10] and obtain a way to express it as a quantum observable. This means that by using this MMD observable as a loss function, IQP-based models can be trained classically efficiently.

Thus, successful tools from classical ML like automatic differentiation and backpropagation can be used in the training of the model. This solves a critical challenge in the optimization of parametrized quantum circuits: indeed, without backpropagation scaling, each estimation of the gradient of the loss function requires as many circuit evaluations as there are parameters, thus making gradient descent very costly as circuits grow in size.

At the same time, in generative learning, the task of deploying the model simply means generating new data samples – in the case of parametrized quantum circuits, this only requires sampling from the circuit through measurement. Crucially, the task of sampling from IQP circuits remains hard classically in general, despite the den Nest algorithm. This means that quantum hardware would likely still be required for the model to be deployed and used.

Interestingly, IQP circuits are not the only circuits with these properties. In particular, discrete variable linear optical quantum computing (DVLOQC) also offers this level of “intermediate complexity”. Indeed, boson sampling is expected to be hard classically [11], while there exist efficient classical algorithms for estimating the expectation value of observables in linear optics [12, 13]. We thus set out to extend this framework to DVLOQC.

In this work, we propose a training procedure for photon-native [14] quantum generative mod-

Alexia Salavrakos: alexia.salavrakos@quandela.com

els based on the MMD and on Gurvits' algorithm for the approximation of probability amplitudes in linear optics. We train our model on datasets that can be represented as fixed Hamming-weight bitstrings, as this corresponds to the natural outputs of a linear optical circuit. In our simulations we train models with up to 16 photons in 256 modes and more than 100 000 parameters in reasonable time on a laptop. We explore initialization strategies as well as different interferometer meshes and parametrizations of the ansatz. Our code framework is available on the MerLin platform [15], Quandela's open-source Python framework for photonic QML.

2 Preliminaries

2.1 Discrete variable linear optical quantum computing

We consider a setup where a source emits single photons which are prepared as Fock states $|s\rangle \in \Phi_{m,n}$, where

$$\Phi_{m,n} = \{|s_1, \dots, s_m\rangle \mid \sum_i s_i = n, s_i \in \{0, \dots, n\}\},$$

with m the number of optical modes and n the number of photons. State $|s\rangle$ is sent as an input to a circuit which is a universal interferometer made of beam-splitters and phase-shifters, implemented for example through the rectangular Clements scheme [16]. Such an interferometer is said to be universal as it can express any $m \times m$ unitary U , i.e. any unitary evolution in the single-particle space where state $|s\rangle$ contains only $n = 1$ photon. When $n \geq 1$, the interferometer applies the operator $\tilde{U} = \varphi(U)$, which is the extension of U on the multi-particle space¹.

At the output of the circuit, there are photon number detectors measuring in the Fock basis of states in $\Phi_{m,n}$, thus producing output arrangements of the form $s' = (s'_1, \dots, s'_m)$, with $\sum_i s'_i = n$ in the lossless case where the number of photons n is conserved. For an input state $|s^{in}\rangle$ and an output state $|s^{out}\rangle$, the corresponding probability amplitude is given by

$$\langle s^{out} | \tilde{U} | s^{in} \rangle = \frac{\text{Perm}(U_{s^{in}, s^{out}})}{\sqrt{\prod_i s_i^{in}! \prod_j s_j^{out}!}}, \quad (1)$$

¹See, e.g. [11] for a description of mapping φ . Note that we adopt the tilde notation for operators acting on the multi-particle space.

where $U_{s^{in}, s^{out}}$ is a submatrix of the single-particle unitary U , formed by taking s_i^{out} times the i th row of U , then s_j^{in} times the j th column of that intermediate matrix.

Sampling from the circuit that prepares the state $\tilde{U} |\psi\rangle$ is a task known as *boson sampling*. Both exact sampling and approximate sampling are expected to be classically hard – provided some conditions on U , as conjectured by Aaronson and Arkhipov [11].

For estimation problems however, the situation is different. In general, an observable on the Fock space is defined as a normal operator \mathcal{Q} that satisfies $\mathcal{Q} = \tilde{U}^\dagger \Lambda \tilde{U}$, where Λ is diagonal in the Fock basis: $\Lambda |s\rangle = \lambda(s) |s\rangle$ [17]. The expectation value of \mathcal{Q} is thus:

$$\begin{aligned} E(\mathcal{Q}) &= \langle \psi | \tilde{U}^\dagger \Lambda \tilde{U} | \psi \rangle = \sum_{s \in \Phi_{m,n}} \lambda(s) P_U(s | \psi) \\ &= \sum_{s \in \Phi_{m,n}} \lambda(s) \|\langle s | \tilde{U} | \psi \rangle\|^2 \\ &= \sum_{s \in \Phi_{m,n}} \lambda(s) \left\| \frac{\text{Perm}(U_{\psi, s})}{\sqrt{\prod_i s_i! \prod_j \psi_j!}} \right\|^2 \end{aligned}$$

for some input state $|\psi\rangle$. Note that \mathcal{Q} is defined to be normal rather than Hermitian which means that the eigenfunction λ can be complex valued.

Now, if we start from an operator defined on the single-particle space $Q = U^\dagger D U$ where U is unitary and $D = \text{diag}(l_1, \dots, l_m)$, then we can map it to an observable \tilde{Q} on the multi-particle space. There, its eigenvalues are given by the products of the l_i via the following eigenfunction:

$$\lambda(s) = \prod_i l_i^{s_i}, \quad (2)$$

where the s_i are the mode occupancy numbers of Fock state $|s\rangle$. We then have the following bound on the singular value of \tilde{Q} : $|\lambda(s)| \leq \max(|l_i|)^n = \|\tilde{Q}\|^n$. Additionally, the expectation value of such an observable can be expressed by a single permanent:

$$E(\tilde{Q}) = \langle \psi | \tilde{Q} | \psi \rangle = \frac{\text{Perm}(Q_{\psi, \psi})}{\sqrt{\prod_i \psi_i! \prod_j \psi_j!}}. \quad (3)$$

Importantly, this quantity can be approximated classically in $O(n^2/\epsilon^2)$ with precision $\pm\epsilon\|\tilde{Q}\|^n$ using Gurvits' algorithm and its generalizations [12, 18]². Hence, if $\|\tilde{Q}\| \leq 1$, the quantity (3) can

²See also [13] for further results on the classical estimation of probabilities and expectation values in DVLOQC, including input Fock states in superposition

be approximated classically *efficiently*. Note that Gurvits' algorithm is based on the Glynn estimator, which for a given $x \in \{-1, 1\}^n$ is defined for an $n \times n$ matrix A as

$$\text{Gly}_x(A) := x_1 \cdots x_n \prod_{i=1}^n (a_{i,1}x_1 + \cdots + a_{i,n}x_n). \quad (4)$$

More precisely, we have that:

$$\text{Per}(A) = \mathbb{E}_{x \in \{-1, 1\}^n} [\text{Gly}_x(A)].$$

2.2 Generative model

Our model is the photonic quantum circuit Born machine (QCBM) described in [19], i.e. a variational quantum generative model based on DVLOQC with n photons and m modes. In a nutshell, the model consists of an input Fock state $|s\rangle$ that goes through a parametrized linear optical interferometer that prepares state $|\psi_\theta\rangle = \tilde{U}_\theta |s\rangle$, which is then measured by the photon detectors. The outputs strings $\mathbf{s}' = (s'_1, \dots, s'_m)$ are the generated data: each measurement output vector \mathbf{s}' is considered to be a sample generated by the model.

The parameters θ of the model are the phases of phase shifters inside the circuit interferometer, which is thus described by an $m \times m$ matrix U_θ . This matrix can be decomposed into different linear optical ansätze: in the case of the rectangular interferometer [16], U_θ is decomposed in a product of $T(\theta_i^j, \theta_i^j)$ matrices that each correspond to a Mach-Zender Interferometer (MZI) element between the j -th and $(j+1)$ -th modes:

$$\begin{pmatrix} 1 & 0 & \cdots & & \cdots & 0 \\ 0 & 1 & & & & \vdots \\ \vdots & & e^{i\theta_i^j} \cos \frac{\theta_i^j}{2} & -\sin \frac{\theta_i^j}{2} & & \vdots \\ & & e^{i\theta_i^j} \sin \frac{\theta_i^j}{2} & \cos \frac{\theta_i^j}{2} & & \vdots \\ \vdots & & & & 1 & 0 \\ 0 & \cdots & & \cdots & 0 & 1 \end{pmatrix}$$

Overall, the resulting U_θ matrix can be expressed as a product of $m(m-1)/2$ such matrices and a diagonal matrix. There is a total of m^2 phases in the interferometer, i.e. m^2 parameters in the model.

As for the learning problem, a target dataset is given which contains N training data samples which should also be of the form $\mathbf{x} = (x_1, \dots, x_m)$.

The goal is to train the model parameters θ so that the samples \mathbf{s}' produced by the model resemble the target samples \mathbf{x} according to a chosen loss function and metrics.

3 Estimating the MMD loss in linear optics

3.1 MMD observable

One such metric used in generative learning is the MMD, which was introduced in the context of classical ML in [10]. It measures a distance between distributions p and q and is expressed as:

$$\begin{aligned} \text{MMD}^2(p, q) &= \mathbb{E}_{\mathbf{x}, \mathbf{y} \sim p} [K(\mathbf{x}, \mathbf{y})] \\ &\quad - 2\mathbb{E}_{\mathbf{x} \sim p, \mathbf{y} \sim q} [K(\mathbf{x}, \mathbf{y})] \\ &\quad + \mathbb{E}_{\mathbf{x}, \mathbf{y} \sim q} [K(\mathbf{x}, \mathbf{y})], \end{aligned} \quad (5)$$

where $K(\mathbf{x}, \mathbf{y})$ is a kernel function. We pick a common kernel choice studied in [9, 6], the Gaussian kernel with bandwidth parameter σ :

$$K_\sigma(\mathbf{x}, \mathbf{y}) = \exp\left(\frac{-\|\mathbf{x} - \mathbf{y}\|^2}{2\sigma^2}\right). \quad (6)$$

Note that another way to write the MMD is the following:

$$\begin{aligned} \text{MMD}^2(p, q) &= \sum_{\mathbf{x}, \mathbf{y} \in \mathcal{X}} p(\mathbf{x})p(\mathbf{y})K(\mathbf{x}, \mathbf{y}) \\ &\quad - 2 \sum_{\mathbf{x}, \mathbf{y} \in \mathcal{X}} p(\mathbf{x})q(\mathbf{y})K(\mathbf{x}, \mathbf{y}) \\ &\quad + \sum_{\mathbf{x}, \mathbf{y} \in \mathcal{X}} q(\mathbf{x})q(\mathbf{y})K(\mathbf{x}, \mathbf{y}). \end{aligned} \quad (7)$$

An important property of the MMD is that it can be computed as an *average over samples drawn from the target and model distributions*, thus making it an implicit loss function for a generative model, as pointed out in [9]. Indeed, it can be obtained by sampling batches of vectors $\mathcal{X} = \{\mathbf{x}_i \sim p\}$ and $\mathcal{Y} = \{\mathbf{y}_j \sim q\}$ and using the following estimator of the MMD^2 which is an unbiased estimator:

$$\begin{aligned} \hat{\text{MMD}}^2(\mathcal{X}, \mathcal{Y}) &= \frac{1}{|\mathcal{X}|(|\mathcal{X}|-1)} \sum_{i \neq j} K(\mathbf{x}_i, \mathbf{x}_j) \\ &\quad - \frac{2}{|\mathcal{X}||\mathcal{Y}|} \sum_{i, j} K(\mathbf{x}_i, \mathbf{y}_j) \\ &\quad + \frac{1}{|\mathcal{Y}|(|\mathcal{Y}|-1)} \sum_{i \neq j} K(\mathbf{y}_i, \mathbf{y}_j). \end{aligned} \quad (8)$$

In [9], the authors highlight that, in QML, each of the three terms in the MMD loss function can be seen as the expectation value of an observable:

$$\mathcal{M}(\rho, \rho') = \text{Tr} \left[O_{\text{MMD}}^{(\sigma)}(\rho \otimes \rho') \right], \quad (9)$$

with:

$$O_{\text{MMD}}^{(\sigma)} = \sum_{x,y} K_{\sigma}(x, y) |x\rangle \langle x| \otimes |y\rangle \langle y|, \quad (10)$$

and where, depending on which term of the MMD is considered, ρ and ρ' can either be the state prepared by the quantum model, or a state representing the classical training data. Then, they show that $O_{\text{MMD}}^{(\sigma)}$ can be rewritten as a sum of Pauli strings $Z^{\mathbf{k}}$, which are tensor products of Pauli and identity operators on m subsystems:

$$Z^{\mathbf{k}} = Z_1^{k_1} \otimes \dots \otimes Z_m^{k_m},$$

where $Z_i^{k_i} = Z_i$ if $k_i = 1$ and $Z_i^{k_i} = \mathbf{I}$ if $k_i = 0$. More precisely, they obtain:

$$O_{\text{MMD}}^{(\sigma)} = \sum_{\mathbf{k}} (1 - p_{\sigma})^{m-|\mathbf{k}|} p_{\sigma}^{|\mathbf{k}|} Z^{\mathbf{k}} \otimes Z^{\mathbf{k}}, \quad (11)$$

where $p_{\sigma} = \frac{1-e^{-\frac{1}{2\sigma^2}}}{2}$ and where $|\mathbf{k}|$ is the Hamming weight of \mathbf{k} . Putting everything together, this means that the MMD loss function amounts to a mixture of expectation values of observables:

$$\text{MMD}^2(p, q) = \mathbb{E}_{\mathbf{k} \sim \mathcal{P}_{\sigma}(\mathbf{k})} \left[(\langle Z^{\mathbf{k}} \rangle_p - \langle Z^{\mathbf{k}} \rangle_q)^2 \right]$$

where \mathbf{k} is distributed according to a product of Bernoulli distributions with probability p_{σ} ,

$$\mathcal{P}_{\sigma}(\mathbf{k}) = (1 - p_{\sigma})^{m-|\mathbf{k}|} p_{\sigma}^{|\mathbf{k}|}.$$

Thus, the MMD loss function can be evaluated by sampling \mathbf{k} vectors and computing the MMD as a sample average.

Now, let us return to linear optics. We define $W^{\mathbf{k}}$ as an operator in the single-particle space as the following diagonal $m \times m$ matrix:

$$W^{\mathbf{k}} = \begin{pmatrix} (-1)^{k_1} & & \\ & \ddots & \\ & & (-1)^{k_m} \end{pmatrix}, \quad (12)$$

and we denote $\tilde{W}^{\mathbf{k}}$ its extension in the multi-particle space. Additionally, we define data domains $\mathcal{X}_{m,n}$ and $\tilde{\mathcal{X}}_{m,n}$ of vectors of size m with fixed Hamming-weight n :

$$\mathcal{X}_{m,n} = \{(x_1, \dots, x_m) \mid \sum_i x_i = n, x_i \in \{0, \dots, n\}\},$$

$$\tilde{\mathcal{X}}_{m,n} = \{(x_1, \dots, x_m) \mid \sum_i x_i = n, x_i \in \{0, 1\}\}.$$

This case of $\tilde{\mathcal{X}}_{m,n}$ where the x_i are limited to 0 and 1 values corresponds to the no-collision regime³ in linear optics, valid when $m \gg n^2$. We can now state our main proposition.

Proposition 1. *The MMD loss function for distributions p, q defined on $\tilde{\mathcal{X}}_{m,n}$ can be computed with the linear optical observable*

$$O_{\text{MMD}, LO}^{(\sigma)} = \sum_{\mathbf{k}} (1 - p_{\sigma})^{m-|\mathbf{k}|} p_{\sigma}^{|\mathbf{k}|} \tilde{W}^{\mathbf{k}} \otimes \tilde{W}^{\mathbf{k}}$$

in the no-collision regime.

Proof. We focus on the term of the MMD where both distributions come from the QCBM, as the classical terms are straightforward. Using expression (7), we wish to show that:

$$\langle \psi_{\theta} | O_{\text{MMD}, LO}^{(\sigma)} | \psi_{\theta} \rangle = \sum_{\mathbf{x}, \mathbf{y} \in \tilde{\mathcal{X}}_{m,n}} q(\mathbf{x}) q(\mathbf{y}) K_{\sigma}(\mathbf{x}, \mathbf{y}) \quad (13)$$

Let us call this term $\text{MMD}_{q_{\theta}, q_{\theta}}$. Since the quantum circuit prepares state $|\psi_{\theta}\rangle = \tilde{U}_{\theta} |s\rangle$, we have that, expanding $O_{\text{MMD}, LO}^{(\sigma)}$:

$$\text{MMD}_{q_{\theta}, q_{\theta}} = \sum_{\mathbf{k}} (1 - p_{\sigma})^{m-|\mathbf{k}|} p_{\sigma}^{|\mathbf{k}|} \cdot \langle s | \tilde{U}_{\theta}^{\dagger} \tilde{W}^{\mathbf{k}} \tilde{U}_{\theta} | s \rangle \langle s | \tilde{U}_{\theta}^{\dagger} \tilde{W}^{\mathbf{k}} \tilde{U}_{\theta} | s \rangle$$

Here,

$$\langle s | \tilde{U}_{\theta}^{\dagger} \tilde{W}^{\mathbf{k}} \tilde{U}_{\theta} | s \rangle = \left(\sum_{x \in \Phi_{m,n}} \lambda^{\mathbf{k}}(x) P_{U_{\theta}}(x|s) \right),$$

and, following equation (2) and the form of $W^{\mathbf{k}}$:

$$\lambda^{\mathbf{k}}(x) = \prod_{i=1}^m \left((-1)^{k_i} \right)^{x_i}.$$

So, the expression becomes:

$$\text{MMD}_{q_{\theta}, q_{\theta}} = \sum_{\mathbf{x}, \mathbf{y} \in \mathcal{X}_{m,n}} q_{\theta}(\mathbf{x}) q_{\theta}(\mathbf{y}) \cdot \sum_{\mathbf{k}} \left((1 - p_{\sigma})^{m-|\mathbf{k}|} p_{\sigma}^{|\mathbf{k}|} \prod_i (-1)^{k_i x_i + k_i y_i} \right)$$

To recover (13), the sum over \mathbf{k} in the above equation must correspond to the kernel $K_{\sigma}(x, y)$.

³This regime is quite relevant in practice in experimental setups, since threshold detectors are more readily available than photon number resolving detectors.

Since the k_i are independent, we can rewrite the sum over \mathbf{k} as:

$$\prod_{i=1}^m \sum_{k_i=0}^1 p_\sigma^{k_i} (1-p_\sigma)^{1-k_i} (-1)^{k_i x_i + k_i y_i},$$

where each factor in the product then equals:

$$(1-p_\sigma) + p_\sigma (-1)^{x_i + y_i}.$$

We have two cases: if $(x_i + y_i) \bmod 2$ is 0, each factor equals 1, and if $(x_i + y_i) \bmod 2$ is 1, each factor equals $1 - 2p_\sigma = e^{-1/2\sigma^2}$. Then, in the full product, the $e^{-1/2\sigma^2}$ will contribute a number of times equal to $\sum_i (x_i + y_i) \bmod 2$, and the rest of the factors will be equal to 1, yielding:

$$\exp\left(-\frac{1}{2\sigma^2} \sum_i ((x_i + y_i) \bmod 2)\right).$$

At this stage, if we assume that we are in the no-collision regime and that $x_i, y_i \in \{0, 1\}$, this is exactly:

$$\exp\left(-\frac{1}{2\sigma^2} \sum_{i=1}^m (x_i - y_i)^2\right),$$

which can also be rewritten in terms of the Hamming distance between \mathbf{x} and \mathbf{y} :

$$\exp\left(-\frac{1}{2\sigma^2} d_H(\mathbf{x}, \mathbf{y})\right).$$

This matches definition (6) of $K_\sigma(\mathbf{x}, \mathbf{y})$, and thus:

$$\text{MMD}_{q_\theta, q_\theta} = \sum_{\mathbf{x}, \mathbf{y} \in \mathcal{X}_{m,n}} q_\theta(\mathbf{x}) q_\theta(\mathbf{y}) K_\sigma(\mathbf{x}, \mathbf{y}).$$

□

Here, it is important to note that, as pointed out in equation (3), because operator $W^{\mathbf{k}}$ is originally defined in the single-particle space, each expectation value $\langle s | \tilde{U}_\theta^\dagger \tilde{W}^{\mathbf{k}} \tilde{U}_\theta | s \rangle$ actually corresponds to a single permanent. This means that the quantum linear optical terms of the MMD can be approximated classically efficiently. We detail the exact procedure to follow in the next section.

3.2 Classical estimation procedure

In [6], the authors define an unbiased MMD estimator for their classical estimation procedure. We can repurpose this estimator straightforwardly here, noting that the part which corresponds to the classical simulation of an IQP

circuit through the den Nest algorithm can be replaced by the classical simulation of a linear optical circuit through the Gurvits algorithm. The method is presented in Figure 1.

For a given set of parameters θ , the time complexity of estimating the MMD loss thus scales as $O(n^2/\epsilon_k^2 \epsilon_z^2)$ if we take $O(1/\epsilon_k^2)$ samples for set \mathcal{A} and $O(1/\epsilon_z^2)$ samples for set \mathcal{Z} , resulting in a precision of $O(\epsilon_z \epsilon_k)$. Additional complexity polynomial in m comes from constructing matrix $Q_{\mathbf{k}, \theta}$.

Regarding precision, we note that the MMD as a classical ML metric is already subject to a limited precision due to the finite number of samples used in its estimation. In our case, the following effects influence the precision: finite number of samples for sets $\mathcal{X}, \mathcal{K}, \mathcal{Z}$ (target dataset, MMD observable, Gurvits estimate), as well as some imprecision when the no-collision assumption is not fully respected. In our numerical tests, we found that these effects did not prevent the MMD to serve its purpose as a loss function, in terms of convergence and numerical stability.

4 Ansätze and initialization strategies in linear optical circuits

4.1 Interferometer choice

Recall that our model, as a photon-native algorithm, directly exploits linear optical elements like beam-splitters and phase shifters instead of the usual hardware-agnostic gates from quantum computing. As explain in Section 2.2, any $m \times m$ unitary U that describes the evolution of a single photon over m modes can be decomposed as a product of Mach-Zender elements defined over two modes. This was first proven by Reck et al. in [20] with a triangular decomposition. The rectangular decomposition often used in hardware was proposed later by Clements et al. in [16].

The rectangular and triangular meshes are not the only options to define universal interferometers, and this question has been studied in several recent works [21, 22, 23, 24]. For instance, the 3-MZI architecture resembles the Clements architecture but adds a third 50:50 beam splitter to each standard MZI, enclosing the external phase shift. There is also the butterfly mesh, based on the sine-cosine decomposition of unitaries, that results in a self-similar pattern of MZIs. Though both meshes are universal, they induce markedly

Sample the following batches:

- $\mathcal{X} = \{\mathbf{x}_i \sim p\}$ with $\mathbf{x}_i \in \{0, 1\}^n$, which are the samples from the target dataset,
- $\mathcal{K} = \{\mathbf{k}_j \sim \mathcal{P}_\sigma\}$ with $\mathbf{k}_j \in \{0, 1\}^n$ to construct the MMD observable, where \mathcal{P}_σ given by $\mathcal{P}_\sigma(\mathbf{k}) = (1 - p_\sigma)^{m-|\mathbf{k}|} p_\sigma^{|\mathbf{k}|}$ with $p_\sigma = \frac{1 - e^{-\frac{1}{2\sigma^2}}}{2}$,
- $\mathcal{Z} = \{\mathbf{z}_l \sim U\}$ with $\mathbf{z}_l \in \{-1, 1\}^n$ sampled uniformly to perform Gurvits' algorithm.

Then, get unbiased estimates of the MMD² with the following formula:

$$\begin{aligned} \widehat{\text{MMD}}^2(\mathcal{X}, \mathcal{K}, \mathcal{Z}, \theta) &= \frac{1}{|\mathcal{K}||\mathcal{Z}|(|\mathcal{Z}|-1)} \sum_{i,j,l \neq j} f(\mathbf{k}_i, \mathbf{z}_j, \theta) f(\mathbf{k}_i, \mathbf{z}_l, \theta) \\ &\quad - \frac{2}{|\mathcal{K}||\mathcal{Z}||\mathcal{X}|} \sum_{i,j,l} f(\mathbf{k}_i, \mathbf{z}_j, \theta) (-1)^{\mathbf{x}_l \cdot \mathbf{k}_i} \\ &\quad + \frac{1}{|\mathcal{K}||\mathcal{X}|(|\mathcal{X}|-1)} \sum_{i,j,l \neq j} (-1)^{\mathbf{x}_j \cdot \mathbf{k}_i} (-1)^{\mathbf{x}_l \cdot \mathbf{k}_i}, \end{aligned} \quad (14)$$

with the Glynn estimator

$$f(\mathbf{k}, \mathbf{z}, \theta) = z_1 \cdots z_n \prod_{i=1}^n (q_{i,1} z_1 + \cdots + q_{i,n} z_n), \quad (15)$$

where the $q_{i,j}$ are the entries of matrix $Q_{\mathbf{k},\theta}^{s,s}$, which is a submatrix of $Q_{\mathbf{k},\theta} = U_\theta^\dagger W^{\mathbf{k}} U_\theta$ formed by taking s_i times the i th row of $Q_{\mathbf{k},\theta}$, then s_j times the j th column of that intermediate matrix, given a choice of input state $|s\rangle$. Matrix $Q_{\mathbf{k},\theta}$ is obtained by multiplying the parametrized unitary U_θ that represents the ansatz with the operator $W^{\mathbf{k}} = \text{diag}((-1)^{k_1}, \dots, (-1)^{k_m})$.

Figure 1: Estimation of the MMD observable.

different sampling densities on $U(N)$ when compared to Reck and Clements schemes: drawing phase shifts from the same region of parameter space during initialization can lead to strong over- and under- representation of different unitaries, depending on the mesh geometry [25].

In addition, we can take another approach and consider a parametrization of an $m \times m$ unitary U which does not directly correspond to hardware, i.e., to an interferometer. This does not cause any issues, since with classical training the model can be trained over those parameters, and when the model is deployed, the trained unitary can be decomposed into any mesh which matches the available hardware. In our code, we implement a parametrization where a vector of real parameters is first mapped to a general complex matrix, on which a QR decomposition is then applied. This parametrization is compatible with

the Haar measure, in the sense that it yields Haar-distributed unitaries when the parameters are sampled from an isotropic Gaussian distribution [26].

4.2 Input state

The choice of input state $|s\rangle$ is, in a way, part of the ansatz choice. Often in linear optics, state $|1 \cdots 10 \cdots 0\rangle$ is selected as an input, but there is no reason why the 1s cannot be placed in any input modes, as long as there is always a maximum of one photon per mode. We treat input state definition as a hyperparameter over which the model can be tuned.

The procedure presented in Figure 1 applies to simple Fock states as input states. However, classical simulation algorithms also exist [13] for Fock states prepared in superposition [27], i.e. for observable estimation in superposition boson

sampling. Additionally, entangled input states of single photons can be produced experimentally, such as caterpillar states [28], which are considered a crucial step in the creation of photonic cluster states [29]. To our knowledge, there are currently no efficient classical algorithms for the estimation of observables in this scenario, which is sometimes referred to as entangled boson sampling. It would be interesting to study the conditions under which classical simulation may be possible. Overall, the use of different input states will allow us to relax the constraint of fixed Hamming weight in the generated data, and would likely improve the expressivity of the model.

4.3 Warm starts and initialization strategies

In both quantum and classical variational algorithms, it is well known that clever initializations can greatly improve the performance of an algorithm [30, 31, 32]. We thus propose initialization strategies which depend on the choice of mesh.

One approach which has been studied in the literature [33, 34] is to consider small-angle or identity initializations. The first strategy that we implement is thus to initialize the unitary close to identity, with small perturbations up to a chosen maximal value. For rectangular interferometers and for butterfly meshes, this means initializing angles ϕ and θ close to 0, while for 3-MZI meshes, ϕ and θ are initialized close to $\pi/2$. For the Haar-compatible parametrization, the unitary matrix is set to identity, and a small perturbation is added to its entries.

We also include in our code framework the option to initialize parameters (or phases) fully at random, where the distribution from which the phases are drawn varies according to the geometry of the chosen mesh.

Then, as a “warm start” strategy, we propose to train the model in several iterations that each correspond to a different bandwidth σ . Indeed, the bandwidth of the MMD determines which orders of correlation contribute most strongly to the MMD: a higher σ will match lower-order operators, and vice-versa. In our simulations, we observed that this strategy could improve the final value of the loss function, although the differences often remained below one of order of magnitude.

5 Datasets and applications

Since our linear optical setup generates fixed Hamming-weight bitstrings, it is natural to aim at modelling fixed Hamming-weight bitstrings, instead of transforming or post-processing the circuit’s output samples. In other words, we make use of the boson sampling inductive bias. This means that data points from the target datasets should be vectors $\mathbf{x} = (x_1, \dots, x_m)$ where $\sum x_i = n$ and $x_i \in \{0, 1\}$. We propose datasets that match this format, and code to prepare or generate them.

5.1 Boson sampling datasets

As a first dataset to test the validity of our method, we generate boson sampling datasets using the Perceval [35] package. In particular, we make use of the CliffordClifford2017 backend based on [36], which is appropriate for sampling simulation. The software implementation allows us to go up to $m = 256$ modes, and we select $n = 16$ photons. Eventually, generating this data classically will not be possible as m and n scale, but we could imagine a learning problem where the data comes from samples obtained on hardware.

5.2 User preference datasets

A type of problem that often comes up in data science concerns user preferences: for example, how does a user rank the films they have seen on a streaming platform, or the objects they have bought on an online marketplace? This data may be used in recommendation systems, or for grouping users in clusters and providing them with different client support or marketing strategies. To match the fixed Hamming-weight bitstrings requirement, we rephrase the question slightly and consider a user’s n favourite elements among a list of m items.

It turns out that a quite specific dataset exists for $m = 100$ and $n = 10$ within PrefLib: a library for preferences [37], which provides 5000 samples of the 10 favourite sushi among a list of 100 sushi options. While this is not exactly an industry-ready use case, we use the opportunity to test our model on a real user preference dataset that remains of reasonable size.

Additionally, we prepared datasets for movie

preference for different m and n based on data from the Netflix prize [38], which was used historically for benchmarking tasks.

5.3 Bioinformatics datasets

Bioinformatics is a field where data often naturally appears in bitstring format, for example to encode DNA, or study the effect of compounds on genes [39, 40]. The Connectivity Map (CMap) is a database created by the Broad Institute [41, 42] that catalogs cellular signatures from perturbations with genetic and pharmacologic perturbagens, i.e. stores a description of how gene expression is affected by such compounds. We create datasets by starting from a raw file of compound responses from the CMap platform [43], selecting a so-called gene universe to work with vectors of length m , then assigning 1s to the n most affected genes, i.e. those that exhibit the largest differential expression for a given compound, while the rest are assigned 0s.

6 Numerical experiments

We implemented the procedure from Figure 1 using Python and JAX. We relied on JAX’s ability to automatically differentiate native Python and Numpy functions to carry out the optimization of the model. As an example, a 2000-step training of a model with $m = 100$ modes and $n = 10$ photons takes about 2 hours to complete on a laptop, with 3 to 4 seconds per step.

We summarise our findings in Figure 2. We compare our models against two classical benchmarks: a simple restricted Boltzmann machine (RBM) like the one used in [6], and a uniform random model that generates fixed Hamming-weight bitstrings. We also include the value of the MMD between two halves of the test set, as a ground truth “test to test” baseline.

We chose the Adam optimizer for gradient descent, and we used Ray Tune [44] for hyperparameter tuning and exploration. In the results displayed in Figure 2, we used our close-to-identity parameter initialization, with perturbation bounded by 0.5 – a value chosen during hyperparameter exploration.

In Figures 2a and 2b, we illustrate the effect of choosing different sizes for sets \mathcal{K} and \mathcal{Z} : in both examples, the loss function decreases smoothly

and reaches a similar value, but the oscillations are more marked when the precision is lower.

In terms of parametrizations, our simulations generally showed that the butterfly and Haar-compatible ansätze yielded a better performance for our model. We show this in Figure 2c for the user preference (sushi) dataset. We subsequently selected the Haar-compatible ansatz in the other simulations displayed in Figure 2.

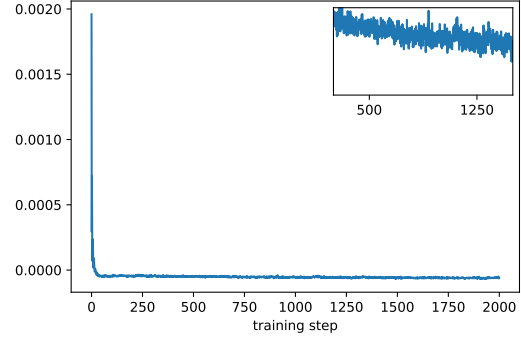
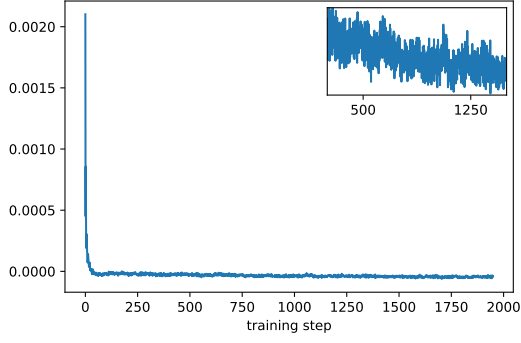
In terms of performance, we observe in Figure 2e that the best performance of the QCBM was for the boson sampling dataset, where it clearly outperforms the classical benchmarks. This could be expected since both the model and the generator that produced the data are boson samplers, so the model naturally has the right inductive bias for such a dataset.

In a sense, this confirms the guideline often repeated in QML, that quantum models are best suited for quantum data, or data obtained from quantum processes [45]. While the boson sampling dataset is not as clearly related to an application as the other datasets, this is an interesting result in its own right, and it indicates that results about quantum data obtained in the qubit picture do apply to the linear-optical or photon-native picture.

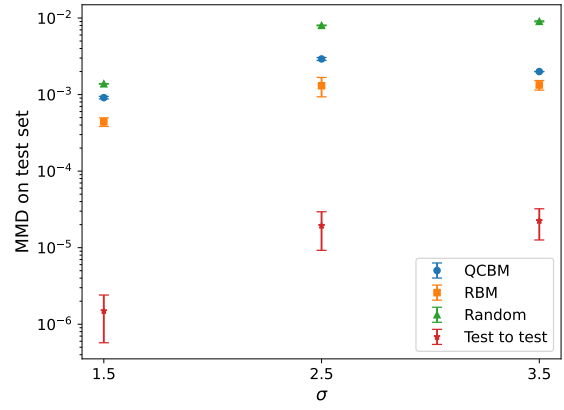
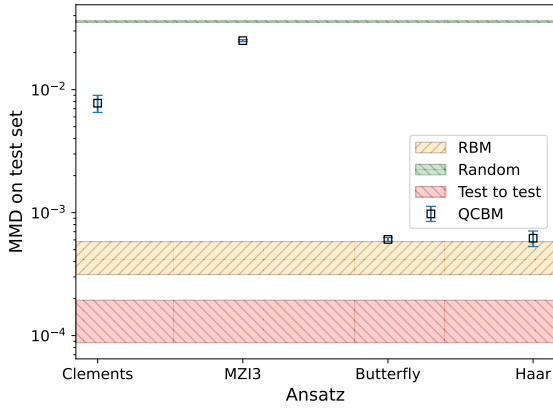
For the user preference as well as the bioinformatics datasets, we observe in Figures 2c, 2d, and 2f a performance that is close to the RBMs. There remains a large gap between the models and the ground truth MMD. It is not clear whether these datasets are simply difficult to learn, or if we could improve the performance of the QCBM – possibly by looking for different kernels that may work better on these datasets and adapting the MMD accordingly, by designing better initialization strategies, or perhaps considering different types of input states. We leave the implementation of these ideas out for future work.

7 Discussion

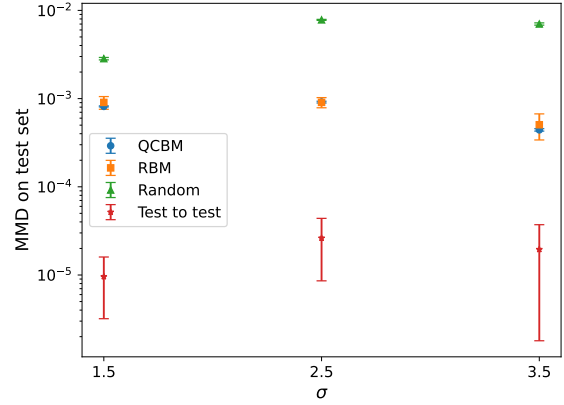
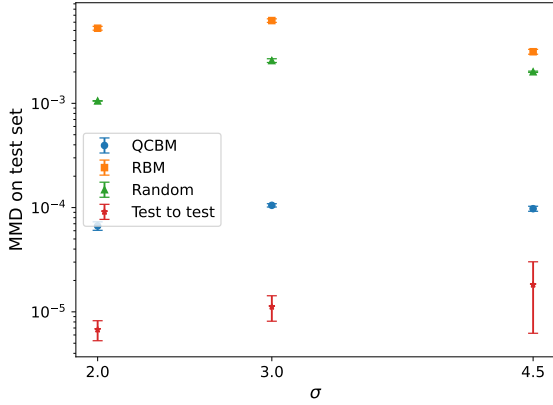
In this work, we present and implement a method to train photon-native quantum generative models efficiently on classical hardware. Importantly, once the model is trained, deploying the model, i.e. sampling from it, coincides with the problem of boson sampling, a task conjectured to be classically hard and thus requiring quantum hardware in general. Of course, the parameters ob-



(a) Boson sampling dataset, $m = 256$, $n = 16$, $\sigma = 3.0$, $|\mathcal{K}| = 2000$, $|\mathcal{Z}| = 2000$. (b) Boson sampling dataset, $m = 256$, $n = 16$, $\sigma = 3.0$, $|\mathcal{K}| = 5000$, $|\mathcal{Z}| = 5000$.



(c) User preference (sushi) dataset, $m = 100$, $n = 10$, for $\sigma = 3.0$ and different ansätze. (d) User preference (movies) dataset, $m = 100$, $n = 15$, for different bandwidths.



(e) Boson sampling dataset, $m = 256$, $n = 16$, for different bandwidths. (f) Bioinformatics dataset, $m = 100$, $n = 10$, for different bandwidths.

Figure 2: Subfigures (a) and (b) compare the MMD loss curve for different sizes of sets \mathcal{K} and \mathcal{Z} from the estimation procedure: when the sets are smaller, the loss has slightly larger variations. Subfigures (c) - (f) display the value of the MMD on the test set for the quantum model and the classical benchmarks, for different datasets. In (c), different choices of interferometers are displayed, and in (d) - (f) different choices of bandwidth σ are shown. The best performance of the quantum model is observed for the boson sampling dataset. Error bars are obtained from repeating the simulations five times each, and in the case of the test-to-test MMD, by shuffling the test set.

tained during training may define unitaries with a structure too specific to prove any complexity-theoretic statement, as was rightfully highlighted recently in [46]; or their structure may even allow for classical simulability of sampling. Nevertheless, this approach allows us to propose a photonic QML algorithm which is both scalable and has a decent chance to escape dequantization.

With this work, we add a new string to the bow of "train on classical, deploy on quantum" methods. Such methods are part of a larger trend of using quantum circuits only where they are strictly necessary within a classical pipeline, as for the "quantum-enhanced classical simulation" paradigm [47, 48, 49] – including recent photonics results in [50]. This trend aligns well with the impressive capabilities of classical computers for certain algorithms: for example, training the circuit classically allows us to use tools like automatic differentiation.

Because of the "train on classical, deploy on quantum" paradigm, we believe that generative learning is a promising area to look for utility of boson sampling. While our work is only a step in that direction, we believe that the datasets and use cases we propose are a good a starting point, and we believe there is potential in looking for more applications in this direction.

Many open questions remain: for instance, it would be interesting to extend our work to the collision case, as well as to different types of input states, as discussed in the text. Additionally, we can certainly explore cases with much larger number of photons and modes if we exploit more significant classical computing resources and high-performance computing.

Moreover, several recent studies have emerged [51, 52, 53, 54] that are either related to the original work of [6] or that build upon it. Integrating their results and approaches into our setup would be highly valuable. In [51], the authors make the model universal and make it possible to train the kernel that appears in the MMD loss function. In [52], the authors study the training of generative models based on correlators, using alternative classical simulation algorithms, allowing them to go beyond the MMD and to consider different ansätze. Finally, in [53], the authors use IQP circuits for graph generation and deploy trained models on superconducting hardware.

Deploying our models on actual devices ap-

pears as a natural next step – in fact, this may be a strength of using linear optical models, as the corresponding circuits are relatively easy to deploy experimentally. Indeed, all required optical components are readily available and interferometers are steadily increasing in size, although the question of noise, in particular photon loss, remains a challenge. Thus, it will be crucial to study our models under noisy conditions [55, 56], and those will certainly imply higher thresholds in terms of the number of photons and modes required to reach an advantage regime for model deployment – in which case, studying the energetic advantage perspective as was done in [57] will be of significant interest.

Acknowledgements

The authors would like to thank Joseph Bowles and Pierre-Emmanuel Emeriau for fruitful discussions. This work has been co-funded by the QuantERA project ResourceQ under the grant agreement ANR-24-QUA2-007-003, and by the EIC Pathfinder program project QUONDEN-SATE under the grant agreement 101130384.

Code availability

Our code is available within Quandela’s MerLin platform, at https://github.com/merlinquantum/generative_classical_training.

References

- [1] Elies Gil-Fuster, Casper Gyurik, Adrian Perez-Salinas, and Vedran Dunjko. On the relation between trainability and dequantization of variational quantum learning models. In *The Thirteenth International Conference on Learning Representations*, 2025.
- [2] Yunchao Liu, Srinivasan Arunachalam, and Kristan Temme. A rigorous and robust quantum speed-up in supervised machine learning. *Nature Physics*, 17(9):1013–1017, July 2021.
- [3] Joseph Bowles, David Wierichs, and Chae-Yeun Park. Backpropagation scaling in parameterised quantum circuits. *Quantum*, 9:1873, October 2025.

- [4] Casper Gyurik and Vedran Dunjko. Exponential separations between classical and quantum learners, 2024.
- [5] Riccardo Molteni, Simon Callum Marshall, and Vedran Dunjko. Quantum machine learning advantages beyond hardness of evaluation. In *The Fourteenth International Conference on Learning Representations*, 2026.
- [6] Erik Recio-Armengol, Shah Nawaz Ahmed, and Joseph Bowles. Train on classical, deploy on quantum: scaling generative quantum machine learning to a thousand qubits. *arXiv:2503.02934*, 2025.
- [7] Dan Shepherd and Michael J. Bremner. Temporally unstructured quantum computation. *Proceedings of the Royal Society A: Mathematical, Physical and Engineering Sciences*, 465(2105):1413–1439, February 2009.
- [8] M. Van den Nest. Simulating quantum computers with probabilistic methods, 2010.
- [9] Manuel S. Rudolph, Sacha Lerch, Supanut Thanasilp, Oriël Kiss, Oxana Shaya, Sofia Vallecorsa, Michele Grossi, and Zoë Holmes. Trainability barriers and opportunities in quantum generative modeling. *npj Quantum Information*, 10(116), 2024.
- [10] Arthur Gretton, Karsten M. Borgwardt, Malte J. Rasch, Bernhard Schölkopf, and Alexander Smola. A kernel two-sample test. *Journal of Machine Learning Research*, 13(25):723–773, 2012.
- [11] Scott Aaronson and Alex Arkhipov. The computational complexity of linear optics. *Proceedings of the forty-third annual ACM symposium on Theory of computing*, pages 333–342, 2011.
- [12] Leonid Gurvits. On the complexity of mixed discriminants and related problems. In Joanna Jędrzejowicz and Andrzej Szepietowski, editors, *Mathematical Foundations of Computer Science 2005*, pages 447–458, Berlin, Heidelberg, 2005. Springer Berlin Heidelberg.
- [13] Youngrong Lim and Changhun Oh. Efficient classical algorithms for linear optical circuits. *arXiv:2502.12882*, 2025.
- [14] Alexia Salavrakos, Nicolas Maring, Pierre-Emmanuel Emeriau, and Shane Mansfield. Photon-native quantum algorithms. *Materials for Quantum Technology*, 5(2):023001, apr 2025.
- [15] Cassandre Notton, Benjamin Stott, Philippe Schoeb, Anthony Walsh, Grégoire Leboucher, Vincent Espitalier, Vassilis Apostolou, Louis-Félix Vigneux, Alexia Salavrakos, and Jean Senellart. Merlin: A discovery engine for photonic and hybrid quantum machine learning, 2026.
- [16] William R. Clements, Peter C. Humphreys, Benjamin J. Metcalf, W. Steven Kolthammer, and Ian A. Walmsley. Optimal design for universal multiport interferometers. *Optica*, 3(12):1460–1465, Dec 2016.
- [17] Giovanni de Felice and Christopher Collett. Differentiation of linear optical circuits, 2024.
- [18] Scott Aaronson and Travis Hance. Generalizing and derandomizing gurvits’s approximation algorithm for the permanent. *Quantum Info. Comput.*, 14(7 & 8):541–559, May 2014.
- [19] Alexia Salavrakos, Tigran Sedrakyan, James Mills, Shane Mansfield, and Rawad Mezher. Error-mitigated photonic quantum circuit born machine. *Physical Review A*, 111(3), March 2025.
- [20] Michael Reck, Anton Zeilinger, Herbert J. Bernstein, and Philip Bertani. Experimental realization of any discrete unitary operator. *Phys. Rev. Lett.*, 73:58–61, Jul 1994.
- [21] Ryan Hamerly, Saumil Bandyopadhyay, and Dirk Englund. Asymptotically fault-tolerant programmable photonics. *Nature Communications*, 13(1), November 2022.
- [22] S. A. Fldzhyan, M. Yu. Saygin, and S. P. Kulik. Optimal design of error-tolerant reprogrammable multiport interferometers. *Opt. Lett.*, 45(9):2632–2635, May 2020.
- [23] Jasvith Raj Basani, Sri Krishna Vadlamani, Saumil Bandyopadhyay, Dirk R. Englund, and Ryan Hamerly. A self-similar sine-cosine fractal architecture for multiport interferometers. In *CLEO 2023*, page JW2A.87. Optica Publishing Group, 2023.

- [24] Mihai Crisan, David A. Carpenter, and Shamsul Arafin. Recurrent multiport interferometers for fault-tolerant programmable photonics. *Opt. Express*, 33(12):24628–24646, Jun 2025.
- [25] Ryan Hamerly, Jasvith Raj Basani, Alexander Sludds, Sri Krishna Vadlamani, and Dirk Englund. Toward the information-theoretic limit of programmable photonics. *APL Photon.*, 10(11):110803, 2025.
- [26] Francesco Mezzadri. How to generate random matrices from the classical compact groups, 2007.
- [27] J. C. Loredó, C. Antón, B. Reznichenko, P. Hilaire, A. Harouri, C. Millet, H. Ollivier, N. Somaschi, L. De Santis, A. Lemaître, I. Sagnes, L. Lanco, A. Auffèves, O. Krebs, and P. Senellart. Generation of non-classical light in a photon-number superposition. *Nature Photonics*, 13(11):803–808, August 2019.
- [28] H. Huet, P. R. Ramesh, S. C. Wein, N. Coste, P. Hilaire, N. Somaschi, M. Morassi, A. Lemaître, I. Sagnes, M. F. Doty, O. Krebs, L. Lanco, D. A. Fioretto, and P. Senellart. Deterministic and reconfigurable graph state generation with a single solid-state quantum emitter. *Nature Communications*, 16(1), May 2025.
- [29] Netanel H. Lindner and Terry Rudolph. Proposal for pulsed on-demand sources of photonic cluster state strings. *Physical Review Letters*, 103(11), September 2009.
- [30] Maciej Skorski, Alessandro Temperoni, and Martin Theobald. Revisiting weight initialization of deep neural networks. In *Proceedings of the 2nd Mathematical and Scientific Machine Learning Conference*, volume 145 of *Proceedings of Machine Learning Research*, pages 1–20. PMLR, 2021.
- [31] Meenal V. Narkhede, Prashant P. Bartakke, and Mukul S. Sutaone. A review on weight initialization strategies for neural networks. *Artificial Intelligence Review*, 54(5):3963–3992, 2021.
- [32] Kaining Zhang, Liu Liu, Min-Hsiu Hsieh, and Dacheng Tao. Escaping from the barren plateau via gaussian initializations in deep variational quantum circuits. In *Proceedings of the 36th International Conference on Neural Information Processing Systems, NIPS ’22*, Red Hook, NY, USA, 2022. Curran Associates Inc.
- [33] Edward Grant, Leonard Wossnig, Mateusz Ostaszewski, and Marcello Benedetti. An initialization strategy for addressing barren plateaus in parametrized quantum circuits. *Quantum*, 3:214, December 2019.
- [34] Yabo Wang, Bo Qi, Chris Ferrie, and Daoyi Dong. Trainability enhancement of parameterized quantum circuits via reduced-domain parameter initialization. *Physical Review Applied*, 22(5), November 2024.
- [35] Nicolas Heurtel, Andreas Fyrrillas, Grégoire de Gliniasty, Raphaël Le Bihan, Sébastien Malherbe, Marceau Pailhas, Eric Bertasi, Boris Bourdoncle, Pierre-Emmanuel Emeriau, Rawad Mezher, Luka Music, Nadia Belabas, Benoît Valiron, Pascale Senellart, Shane Mansfield, and Jean Senellart. Perceval: A software platform for discrete variable photonic quantum computing. *Quantum*, 7:931, feb 2023.
- [36] Peter Clifford and Raphaël Clifford. *The Classical Complexity of Boson Sampling*, pages 146–155.
- [37] Nicholas Mattei and Toby Walsh. Preflib: A library for preferences <http://www.preflib.org>. In Patrice Perny, Marc Pirlot, and Alexis Tsoukiàs, editors, *Algorithmic Decision Theory*, pages 259–270, Berlin, Heidelberg, 2013. Springer Berlin Heidelberg.
- [38] James Bennett and Stan Lanning. The netflix prize. In *Proceedings of the KDD Cup Workshop 2007*, pages 3–6, New York, August 2007. ACM.
- [39] Camille Moeckel, Manvita Mareboina, Maxwell A. Konnaris, Candace S.Y. Chan, Ioannis Mouratidis, Austin Montgomery, Nikol Chantzi, Georgios A. Pavlopoulos, and Ilias Georgakopoulos-Soares. A survey of k-mer methods and applications in bioinformatics. *Computational and Structural Biotechnology Journal*, 23:2289–2303, 2024.
- [40] Yunfei Gao and Albert No. Efficient and low-complexity variable-to-variable length cod-

- ing for dna storage. *BMC Bioinformatics*, 25(1):320, 2024.
- [41] Justin Lamb, Emily D. Crawford, David Peck, Joshua W. Modell, Irene C. Blat, Matthew J. Wrobel, Jim Lerner, Jean-Philippe Brunet, Aravind Subramanian, Kenneth N. Ross, Michael Reich, Haley Hieronymus, Guo Wei, Scott A. Armstrong, Stephen J. Haggarty, Paul A. Clemons, Ru Wei, Steven A. Carr, Eric S. Lander, and Todd R. Golub. The connectivity map: Using gene-expression signatures to connect small molecules, genes, and disease. *Science*, 313(5795):1929–1935, 2006.
- [42] Aravind Subramanian, Rajiv Narayan, Steven M. Corsello, David D. Peck, Ted E. Natoli, Xiaodong Lu, Joshua Gould, John F. Davis, Andrew A. Tubelli, Jacob K. Asiedu, David L. Lahr, Jodi E. Hirschman, Zihan Liu, Melanie Donahue, Bina Julian, Mariya Khan, David Wadden, Ian C. Smith, Daniel Lam, Arthur Liberzon, Courtney Toder, Mukta Bagul, Marek Orzechowski, Oana M. Enache, Federica Piccioni, Sarah A. Johnson, Nicholas J. Lyons, Alice H. Berger, Alykhan F. Shamji, Angela N. Brooks, Anita Vrcic, Corey Flynn, Jacqueline Rosains, David Y. Takeda, Roger Hu, Desiree Davison, Justin Lamb, Kristin Ardlie, Larson Hogstrom, Peyton Greenside, Nathanael S. Gray, Paul A. Clemons, Serena Silver, Xiaoyun Wu, Wen-Ning Zhao, Willis Read-Button, Xiaohua Wu, Stephen J. Haggarty, Lucienne V. Ronco, Jesse S. Boehm, Stuart L. Schreiber, John G. Doench, Joshua A. Bittker, David E. Root, Bang Wong, and Todd R. Golub. A next generation connectivity map: L1000 platform and the first 1,000,000 profiles. *Cell*, 171(6):1437–1452.e17, 2017.
- [43] Clue — connectivity map data portal. <https://clue.io/>, 2025. Accessed: 2025-10-30.
- [44] Richard Liaw, Eric Liang, Robert Nishihara, Philipp Moritz, Joseph E. Gonzalez, and Ion Stoica. Tune: A research platform for distributed model selection and training, 2018.
- [45] Hsin-Yuan Huang, Michael Broughton, Masoud Mohseni, Ryan Babbush, Sergio Boixo, Hartmut Neven, and Jarrod R. McClean. Power of data in quantum machine learning. *Nature Communications*, 12(1), May 2021.
- [46] Sabrina Herbst, Ivona Brandić, and Adrián Pérez-Salinas. Limits of quantum generative models with classical sampling hardness, 2025.
- [47] M. Cerezo, Martin Larocca, Diego García-Martín, N. L. Diaz, Paolo Braccia, Enrico Fontana, Manuel S. Rudolph, Pablo Bermejo, Aroosa Ijaz, Supanut Thanasilp, Eric R. Anschuetz, and Zoë Holmes. Does provable absence of barren plateaus imply classical simulability? *Nature Communications*, 16(1), August 2025.
- [48] Zoltán Zimborás, Bálint Koczor, Zoë Holmes, Elsi-Mari Borrelli, András Gilyén, Hsin-Yuan Huang, Zhenyu Cai, Antonio Acín, Leandro Aolita, Leonardo Banchi, Fernando G. S. L. Brandão, Daniel Cavalcanti, Toby Cubitt, Sergey N. Filippov, Guillermo García-Pérez, John Goold, Orsolya Kálmán, Elica Kyoseva, Matteo A. C. Rossi, Boris Sokolov, Ivano Tavernelli, and Sabrina Maniscalco. Myths around quantum computation before full fault tolerance: What no-go theorems rule out and what they don’t, 2025.
- [49] Hsin-Yuan Huang, Michael Broughton, Jordan Cotler, Sitan Chen, Jerry Li, Masoud Mohseni, Hartmut Neven, Ryan Babbush, Richard Kueng, John Preskill, and Jarrod R. McClean. Quantum advantage in learning from experiments. *Science*, 376(6598):1182–1186, June 2022.
- [50] Hugo Thomas, Ulysse Chabaud, and Pierre-Emmanuel Emeriau. Shedding light on classical shadows: learning photonic quantum states, 2025.
- [51] Andrii Kurkin, Kevin Shen, Susanne Pielawa, Hao Wang, and Vedran Dunjko. Universality and kernel-adaptive training for classically trained, quantum-deployed generative models, 2025.
- [52] Mario Herrero-Gonzalez, Brian Coyle, Kieran McDowall, Ross Grassie, Sjoerd Beentjes, Ava Khamseh, and Elham Kashefi. The born ultimatum: Conditions for classical surrogation of quantum generative models with correlators, 2025.

- [53] Oriol Balló-Gimbernat, Marcos Arroyo-Sánchez, Paula García-Molina, Adan Garriga, and Fernando Vilarino. Shallow iqpcircuit and graph generation, 2025.
- [54] Bence Bakó, Zoltán Kolarovszki, and Zoltán Zimborás. Fermionic born machines: Classical training of quantum generative models based on fermion sampling, 2025.
- [55] Scott Aaronson and Daniel J. Brod. Boson-sampling with lost photons. *Physical Review A*, 93(1), January 2016.
- [56] Raúl García-Patrón, Jelmer J. Renema, and Valery Shchesnovich. Simulating boson sampling in lossy architectures. *Quantum*, 3:169, August 2019.
- [57] Ariane Soret, Nessim Dridi, Stephen C. Wein, Valérian Giesz, Shane Mansfield, and Pierre-Emmanuel Emeriau. Quantum energetic advantage before computational advantage in boson sampling, 2026.